

See discussions, stats, and author profiles for this publication at: <https://www.researchgate.net/publication/260311950>

Size-Dependent Anodic Dissolution of Water-Soluble Palladium Nanoparticles

ARTICLE *in* THE JOURNAL OF PHYSICAL CHEMISTRY C · NOVEMBER 2013

Impact Factor: 4.77 · DOI: 10.1021/jp408394h

CITATIONS

4

READS

54

1 AUTHOR:



Ashok Kumar

Arizona State University

6 PUBLICATIONS 48 CITATIONS

[SEE PROFILE](#)

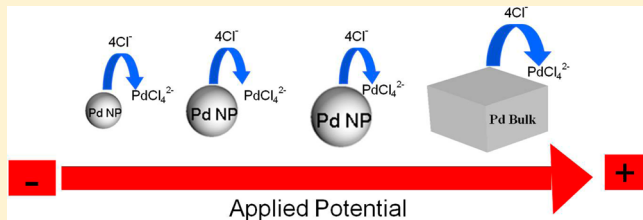
Size-Dependent Anodic Dissolution of Water-Soluble Palladium Nanoparticles

Ashok Kumar and Daniel A. Buttry*

Department of Chemistry and Biochemistry, Arizona State University, Tempe, Arizona 85287-1604, United States

Supporting Information

ABSTRACT: 2,2'-Bicinchoninic acid-capped palladium nanoparticles (Pd-BCA NPs) were synthesized using a one-pot chemical reduction route. Monodisperse Pd-BCA NPs of different size ranges were obtained using a purification technique employing low molecular weight cutoff centrifuge filters. Size-dependent anodic dissolution of Pd-BCA NPs was studied in 0.1 M HClO₄ containing 10 mM NaCl. Experimental data were shown to be in excellent agreement with theoretical values calculated using the Plieth model. For Pd NPs with 1.0 nm diameter, the oxidation was shifted to less positive potentials by over a third of a volt, representing substantial destabilization of the NP due to its small size.



INTRODUCTION

Metal NPs have been studied extensively because of their interesting optical, electronic, catalytic, and magnetic properties as compared to bulk materials, making them an ideal candidate for a variety of applications.^{1–6} A variety of studies have addressed the stability of NPs against aggregation, structural transformations, oxidation, and dissolution.^{7–11} An especially important issue is the stability of metal NPs toward anodic dissolution, given the broad range of electrocatalytic applications that have been investigated for metal NPs. Plieth used thermodynamics to theoretically predict the size dependence of the dissolution potential of metal NPs. According to that model, NP stability toward oxidation should decrease as NP size decreases, producing a negative shift in dissolution potential with decrease in size.¹² This results from the increasing contribution of surface energy to the overall NP stability as size decreases. Data consistent with Plieth's theory were demonstrated by Zamborini et al. with silver and gold nanoparticles.^{13–15} Also, Tang et al. studied the dissolution of Pt NPs using scanning tunneling microscopy and showed smaller particles ($d < 4$ nm) dissolve at lower potential compared to the bulk metal redox potential.^{16,17} They used a more correct model involving the surface stress of both the metal and metal oxide interfaces for the Pt case. As expected, size-dependent shifts in dissolution potential were not observed when Compton and co-workers studied much larger Ag NPs in the 25–100 nm diameter range.¹⁸ These NPs behave as bulk metal and would not be expected to show a size-dependent oxidation potential influenced by surface stress. Two other groups have reported higher dissolution potential for metal nanoparticles as compared to the bulk metal; these results remain unexplained.^{19,20}

The Compton and Zamborini studies also confirmed theoretical work by Brainina et al., who studied the effect of

surface coverage on the oxidation potential of nanoparticles.²¹ They showed that at low scan rates and with relatively fast electron transfer kinetics the peak potentials reflect true thermodynamic oxidation potentials. These conditions remove the influence of overlapping diffusion profiles for the dissolved metal ions produced from the dissolution process and constitute the approach used here.

Increasing interest in Pd and its alloys for electrocatalytic and other applications has motivated us to develop a new synthetic approach for producing Pd NPs. Previous solution-based studies demonstrated using a variety of electrochemical techniques on water-soluble palladium nanoparticles to determine electron transfer rates.²² The synthetic method is modeled after previously published methods for Au and Ag NPs capped with the nucleoside adenosine triphosphate.^{23,24} This method produces water-soluble metal NPs that are isolable as solids, allowing storage and redissolution. The ATP capping ligand binds at the metal NP surface via its nitrogen functional groups. Reasoning by analogy to older work by Schmid and co-workers on production of Pd NPs (so-called “giant clusters”) with phenanthroline capping ligands, a new synthesis of water-soluble Pd NPs is reported here that uses bicinchoninic acid (BCA) as the capping ligand (Scheme 1).²⁵ These BCA-capped palladium nanoparticles (Pd-BCA NPs) are easily synthesized, storable as solids, water-soluble, and provide an attractive platform for electrochemical and other investigations. We report here the synthesis, characterization, and size-dependent anodic dissolution behavior of these NPs. The general approach for the study involved synthesis followed by size fractionation using centrifuge filters typically employed for

Received: August 21, 2013

Revised: November 6, 2013

Published: November 19, 2013

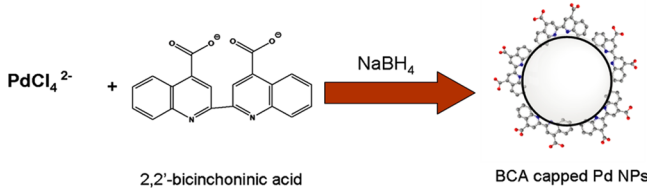


ACS Publications

© 2013 American Chemical Society

26783

dx.doi.org/10.1021/jp408394h | J. Phys. Chem. C 2013, 117, 26783–26789

Scheme 1. Synthesis Scheme of BCA-Capped Pd NPs

size-based protein purification. The different size fractions of Pd-BCA NPs were characterized using powder X-ray diffraction (P-XRD) and transmission electron microscopy (TEM). Size-dependent dissolution studies were performed with drop-cast Pd-BCA NPs trapped by Nafion on a glassy carbon electrode (GCE). The anodic dissolution results are seen to be in excellent agreement with predictions by the Plieth model.

EXPERIMENTAL METHODS

Palladium(II) chloride (PdCl₂, 99%) and sodium borohydride (NaBH₄, 99.9%) were purchased from Sigma-Aldrich, and 2,2'-bicinchoninic acid dipotassium salt hydrate (K₂BCA, >98%) was purchased from TCI America. All reagents were used as obtained. Water of resistivity 18.3 MΩ (Millipore MQ Reference) was used to prepare all the solutions.

Palladium Nanoparticle Synthesis. In the synthesis of water-soluble BCA-Pd NPs, the molar ratio Pd:BCA:BH₄⁻ has a strong influence on the size and stability of the NPs. For the present study, the Pd:BCA:BH₄⁻ molar ratio was mostly held constant at 1:5:10, though a few other sets of ratios were examined. In a typical 1:5:10 synthesis, 6.0 mL of 10 mM H₂PdCl₄ (produced by dissolution of PdCl₂ in dilute HCl) was stirred with 6.0 mL of 50 mM K₂BCA and 222.0 mL of water under nitrogen for 30 min. To this solution (pH ~8), 6.0 mL of freshly prepared 100 mM NaBH₄ (in nitrogen-saturated water) was rapidly added while stirring. The solution with final Pd concentration of 250 μM turned dark purple and then finally brown after the addition of NaBH₄, indicating the reduction of H₂PdCl₄ to Pd NPs capped by BCA. The solution was further stirred for 4 h under nitrogen for complete growth of the nanoparticles. To obtain solid Pd-BCA NPs, the solution was reduced in volume to ~3 mL using a rotary evaporator at 37 °C, and then the NPs were precipitated with ~1 mL of isopropanol. Solid nanoparticles were isolated by centrifugation for 15 min at 5000 rpm. The isolated nanoparticles were dried under nitrogen and redispersed in ~2 mL of water, after which they were reprecipitated using isopropanol. The process of precipitation, centrifugation, and drying under nitrogen was repeated three times to obtain pure BCA-Pd NPs free of excess BCA, which were then dried and stored. This precipitation–centrifugation method was preferred over dialysis because it was considerably faster. NP purity was not determined explicitly, but size distributions were determined by TEM (see below).

A sample containing much larger Pd NPs, with mean diameter in the range 50–100 nm, was also prepared. These NPs were prepared by using a weak reducing agent (ascorbic acid) instead of sodium borohydride. For a bulk Pd sample, 6.0 mL of 10 mM H₂PdCl₄ was stirred with 6.0 mL of 50 mM K₂BCA and 32.0 mL of water under nitrogen for 30 min. To this solution, 6.0 mL of freshly prepared 100 mM ascorbic acid (in nitrogen-saturated water) was rapidly added while stirring. The solution was centrifuged at 5000 rpm to obtain a

precipitate of large Pd NPs, which was redispersed in fresh MQ water. This step was repeated five times to separate free ligands from BCA-capped Pd NPs. This “bulk” sample was used to obtain the oxidation potential for a bulk Pd sample free of size effects, since there should be no influence of size in this range of diameters.

Size Selection of Synthesized BCA-Capped Palladium Nanoparticles.

Synthesis of Pd NPs with different sizes can be achieved by controlling either nucleation or growth of the nanoparticles through control of the BCA to Pd ratio (to control growth) and NaBH₄ to Pd ratio (to control nucleation). However, strict control of size is difficult, especially with regard to the population of outliers (small numbers of NPs well outside of the main population distribution). This is an important point, since even a small number of NPs significantly larger than the main population can substantially skew the electrochemical results because of their potentially much larger electrochemical charge for anodic dissolution. Thus, in the present case, rather than attempting to achieve monodispersity in the size of the NPs through control of the synthetic conditions, we chose to use a size-base separation approach employing centrifuge filters typically used for size-based protein purification (Amicon Ultra-4 Centrifugal Filter Units-Millipore, available in 3K, 10K, 30K, 50K, and 100K sizes). Thus, for size selection the initially synthesized Pd-BCA NP solution (1Pd:5BCA:10BH₄⁻) was concentrated to ~10 mL using a rotatory evaporator. This solution was passed through a 0.1 μm syringe filter to remove any aggregated particles. The obtained solution was then passed through a series of centrifuge filters of different MWCO (molecular weight cutoff) values, with intermediate separation of the filtrate (containing smaller NPs) from the supernatant (containing larger NPs). This allowed size-based separation of the NPs within certain range limits defined by the characteristics of the filters. For example, a typical separation started with centrifugation through a 100 kDa filter at 10 000 rpm for 5 min. The supernatant was collected and labeled as 100 kDa sample. The filtrate obtained was then passed through 30 kDa filter, and the supernatant was labeled as 30 kDa sample. Finally, the filtrate of the second centrifugation step was passed through a 3 kDa filter at 12 000 rpm for 15 min to obtain a 3 kDa sample. All filtered samples were further diluted using MQ water and stored at 4 °C to avoid any agglomeration. The sizes and histograms of the BCA-Pd NPs obtained from this separation method were determined using TEM and will be shown below. The 3K, 30K, and 1000K sizes gave the best resolution, so those are reported here.

Characterization. X-ray diffraction of the solid BCA-Pd NPs was carried out on a Siemens D 5000 X-ray diffractometer using the Cu Kα radiation of 1.541 Å wavelength for 2θ values ranging between 10° and 90° and a scan rate of 2.5°/min. To prepare sample for powder X-ray diffraction, Pd-BCA NPs solutions of different sizes were dried on sample holders under nitrogen. Transmission electron microscopy measurements were carried out using a Phillips CM12 microscope, and HRTEM measurements were done using a JEOL 2010F operated at 80 and 200 kV. TEM samples were prepared by drop-coating 5.0 μL of a dilute sonicated solution of the BCA-Pd NPs onto a Formvar-coated 400 mesh copper grid (Ted Pella Inc.), which was then allowed to dry for 4 h. Histograms were obtained by selecting an area and counting 100 particles from that area.

Electrochemical Measurements. All electrochemical measurements were carried out on a CHI760c potentiostat. Ag/AgCl saturated with 1 M NaCl was used as the reference electrode, while a spiral Pt wire was used as a counter electrode. Glassy carbon electrode (GCE), 3 mm in diameter, was used as a working electrode after polishing consecutively on 1, 0.3, and 0.05 μm Alumina powder for 5 min each and then sonicated for 10 min in MQ water (Millipore) followed by drying under nitrogen flow. Nitrogen was purged through all solutions before electrochemical measurements. For size-dependent electrochemical studies a drop of a solution containing Pd-BCA NPs evaporated on a clean GCE and dried very slowly under nitrogen using an inverted beaker to attain uniform coverage. The NPs were entrapped at the surface by casting a film of Nafion from a 1.0% solution. The Nafion solution was allowed to dry slowly. This method gave surface coverages that were reproducible to roughly 10–20%. Other polymers, such as polyvinylpyrrolidone, were examined for entrapment. However, Nafion produced superior results. The Nafion-entrapped NPs were stable toward extended soaking in electrolyte (i.e., there was no NP dissolution of NP detachment), as expected based on previous reports of this method.²⁶ Electrochemical dissolution studies were performed using linear sweep voltammetry in 0.1 M HClO_4 containing 0.01 M NaCl. Control experiments were done using a glassy carbon electrode coated with Nafion. No redox peaks were observed when Nafion-coated glassy carbon electrodes without Pd-BCA NPs were used. The 50 nm diameter “bulk” Pd NP samples were used to calibrate the oxidation potential for bulk Pd under the specific conditions of the experiment (i.e., to account for reference electrode offsets, junction potentials, any influence from capping ligands, Nafion entrapment, etc.). See Figure S1 in the Supporting Information for TEM images of this sample. Larger Pd particles were used in preference to a pure Pd electrode so that well-defined LSV peaks could be obtained for direct comparison to the LSV data for the BCA-Pd NPs. The dissolution experiments were reproduced three times for the smallest NP sample with average size 1.0 ± 0.3 nm, whereas for other samples it was reproduced seven times to give adequate statistics.

RESULTS AND DISCUSSION

P-XRD scans of various Pd-BCA NPs are shown in Figure 1. The P-XRD of the “bulk” control sample shows peaks near 40° , 46° , 68° , 82° , and 86° , corresponding to the (111), (200), (220), (311), and (222) planes of the face-centered cubic (fcc) crystal structure of palladium.²⁷ As compared to this sample, the Pd-BCA NPs samples showed a broadening of peaks with decreasing size and a reduction in intensity of the higher 2Θ angles, as reported in the literature for other Pd NPs.²⁸ Prior to any size fractionation, the Pd-BCA NPs showed peaks at 39.5° , 67.4° , and 81.2° , corresponding to the (111), (220), and (311) planes. The large fraction of small sized nanoparticles in this “as-synthesized” sample caused the peak at 39.5° to broaden and obscure the peak at 46° corresponding to the (200) plane. This peak reappeared in the diffraction scan of the 100 kDa sample, which was obtained after separating smaller sized nanoparticles from synthesized Pd-BCA NPs using centrifuge filters. The peak broadening becomes more severe for the 30 kDa sample, and the 3 kDa sample shows only a hint of a peak near 40° . These results are consistent with a very significant reduction in the NP size as lower MWCO filters are used for size fractionation. Debye–Scherrer analysis also was used for

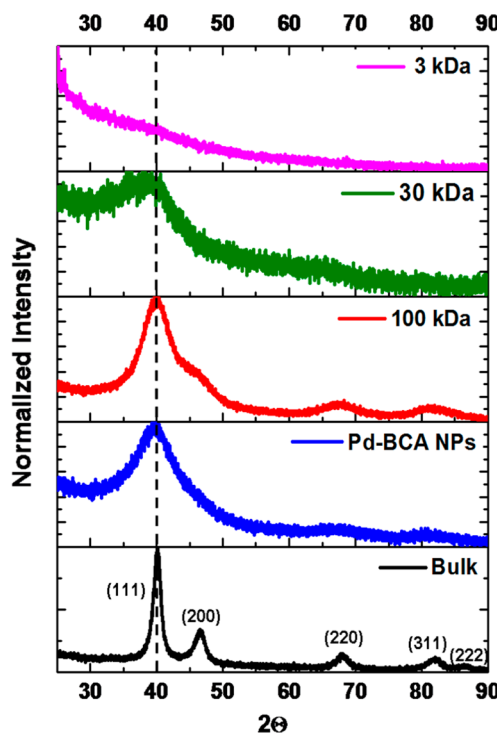


Figure 1. Powder X-ray diffraction for Pd-BCA NPs samples of varying size used for size-dependent anodic dissolution studies, normalized to maximum intensity.

size estimation from peak broadening; the estimated diameters are given in Table 1.

Table 1. Structural and Electrochemical Data for Pd-BCA NPs

sample	mean diam (nm) TEM	estimated mean diam (nm) XRD	lattice param (Å)	theor E_0 (mV)	exptl E_0 (mV)
bulk	98 ± 38	20	3.90	NA	700 ± 14
100 kDa sup	3.2 ± 0.9	3.0	3.93	586	570 ± 10
30 kDa sup	1.5 ± 0.3	1.0	4.03	456	467 ± 12
3 kDa sup	1.0 ± 0.3	NA	>4.03	334	343 ± 15

In addition to peak broadening, decreasing NP size also led to a shift in the peak position to smaller angle showing an increase in lattice parameter. The value for the d -spacing obtained from the (111) peak is 2.25 Å for the “bulk” sample, and the 100 kDa sample and then appears to increase to 2.36 Å for the 30 kDa NPs. A reliable d -value could not be obtained for the 3 kDa sample because of the breadth of the peak.

Previous reports have discussed changes in the lattice parameter with size for Pd NPs.^{29–31} Theoretically, nanoparticles are expected to show lattice contraction with a decrease in size because of an increase in surface stress. This has been observed for a variety of different metal NPs, except palladium which sometimes shows lattice expansion for smaller NPs.^{32–35} For the case of Pd, dilation of the lattice with decrease in size has been explained by structural changes induced by surface oxidation or incorporation of hydrogen, carbon, or oxygen into the lattice.^{36–38} In the present case, these effects should not influence the experimental determination of the oxidation potential since the NPs are held at

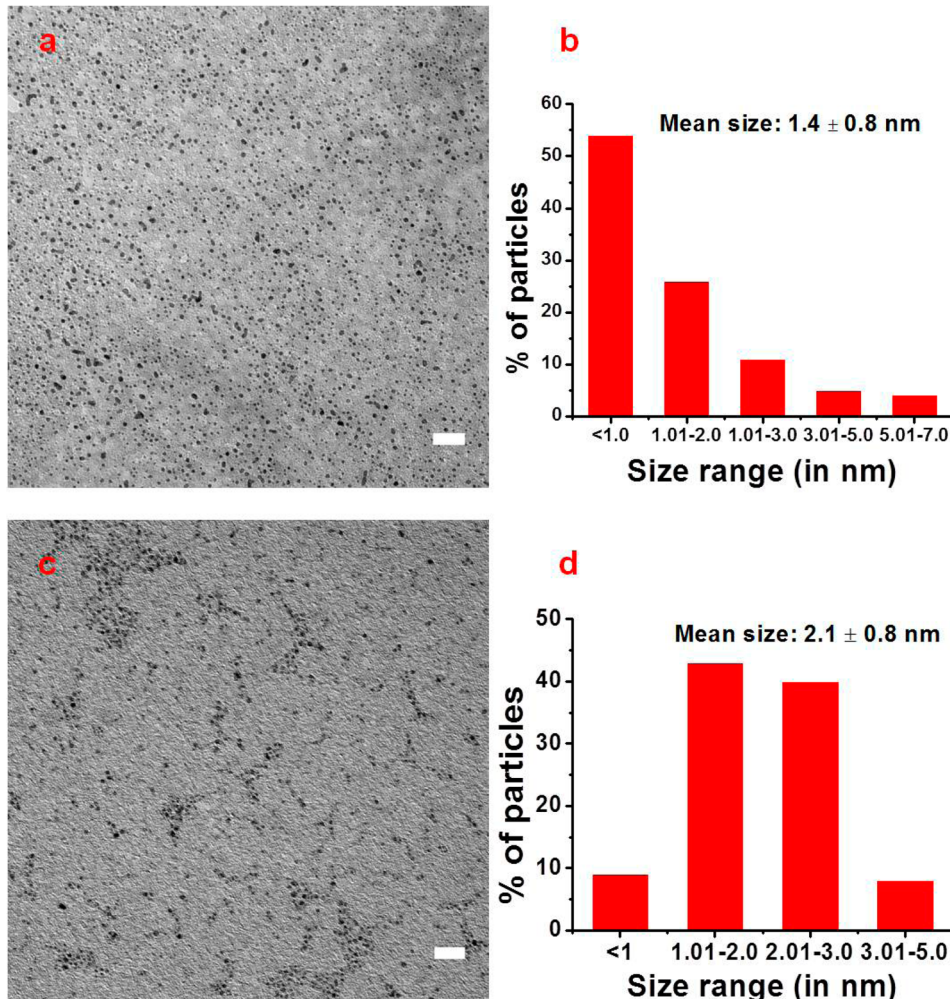


Figure 2. TEM micrograph of BCA-stabilized water-soluble palladium nanoarticles synthesized under (a) higher (Pd:BCA:BH₄⁻ of 1:5:10) and (c) lower (Pd:BCA:BH₄⁻ of 1:1:10) ligand ratio. Nanoparticles are observed as black circles scattered across the mesh grid (scale bar = 20 nm).

negative potentials prior to the anodic scans used in the determination (see below), maintaining the Pd NPs in their metallic state.

TEM images of BCA-Pd NPs produced using a few different Pd:BCA:BH₄⁻ molar ratios are shown in Figure 2. At a lower BCA ratio (Pd:BCA:BH₄⁻ of 1:1:10) NPs of average diameter 2.1 ± 0.8 nm were obtained. There is also some evidence for aggregation for these NPs in the EM images, consistent with less efficient capping at the lower BCA ratio. In contrast, a higher BCA ratio (Pd:BCA:BH₄⁻ of 1:5:10) produced smaller particles of average diameter 1.4 ± 0.8 nm as expected (see Figure S1 in the Supporting Information for TEM images showing larger views of the samples). At higher ratios of BH₄⁻, smaller particles along with several aggregated particles were obtained (see Figure S2 in the Supporting Information for TEM). Thus, the trends in size and aggregation behavior follow the expected behavior for a nucleation and growth mechanism.³⁹

For all of the sizes described, the accompanying size histograms show that the samples are fairly polydisperse. These experiments suggested that it would be challenging to obtain sufficiently monodisperse Pd-BCA NPs for size-dependent studies by varying synthetic conditions alone. Thus, size fractionation using a select range of MWCO centrifuge filters was used. Based on its smaller mean diameter

and sample stability, a sample produced using the 1:5:10 molar ratio was used for the size fractionation process. As described in the Experimental Methods section, these NPs were separated into different size ranges by successively centrifuging through centrifuge filters of MWCO of 100, 30, and 3 kDa. TEM images of Pd-BCA NPs obtained after size fractionation are shown in Figure 3. The 100, 30, and 3 kDa Pd-BCA NPs had an average diameter of 3.2 ± 0.9, 1.5 ± 0.3, and 1.0 ± 0.3 nm, respectively. The obtained fractions were reasonably monodisperse, as shown in the histograms. These samples were then used in anodic dissolution experiments to explore the size dependence of oxidation.

Linear sweep voltammograms (LSVs) of anodic dissolution of Pd-BCA NPs of different sizes entrapped on a glassy carbon surface are shown in Figure 4. Voltammetric scans were done from -0.2 to 1.0 V in 0.1 M HClO₄ containing 10 mM NaCl at 1 mV/s. The difference between the peak currents represents typical variability between different NP samples with different size ranges and does not affect the analysis. The low scan rate ensured the experimental conditions would provide thermodynamic oxidation potentials from the LSV peak potentials, as predicted by Brainina and validated in experiments by Compton and co-workers and Zamborini and co-workers.^{13–15,18,21} To ensure the dissolution process was complete, another LSV was recorded after the first dissolution scan using

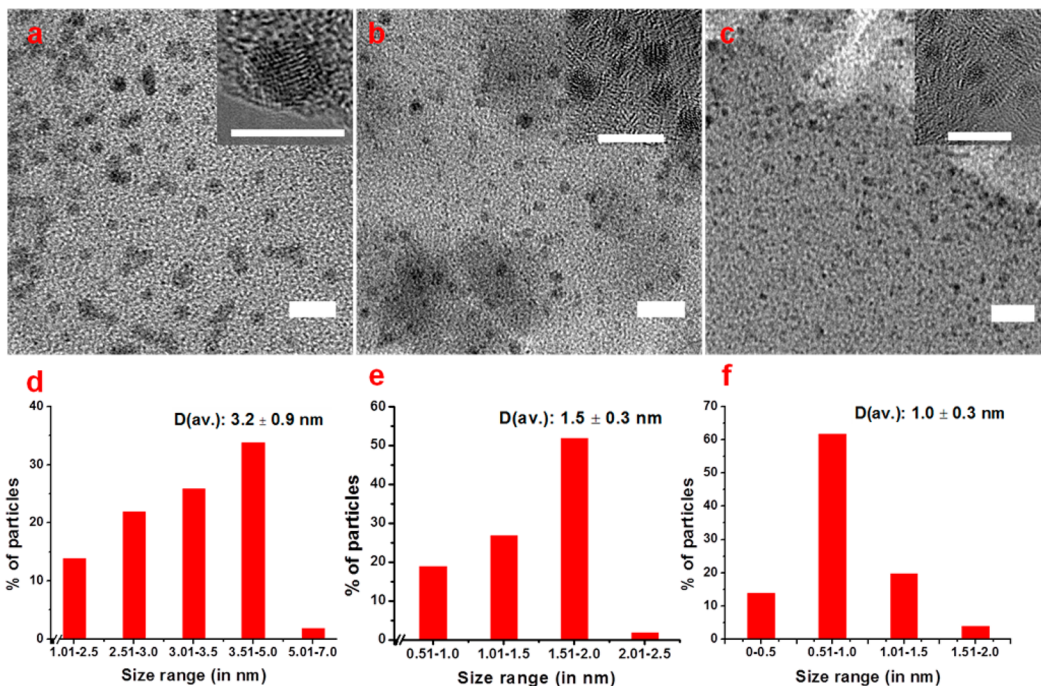


Figure 3. Low-resolution TEM (scale bar = 10 nm) and high-resolution TEM (inset, scale bar = 5 nm) of water-soluble Pd-BCA NPs (Pd:BCA:BH₄⁻ of 1:5:10) purified using centrifugation filters: (a) supernatant of 100 kDa, (b) supernatant of 30 kDa, and (c) supernatant of 3 kDa.

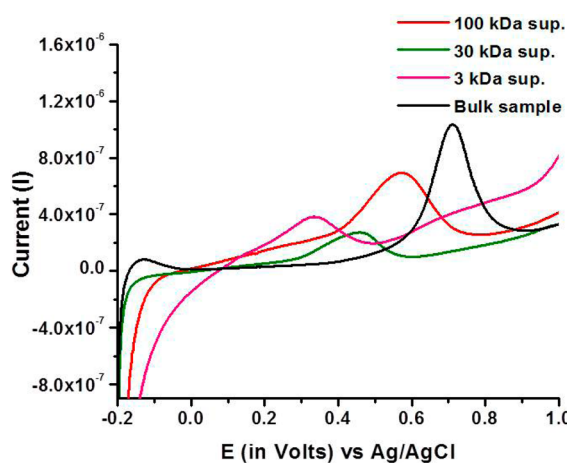


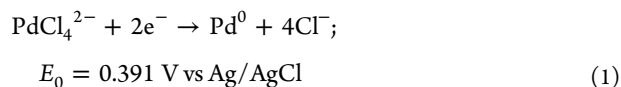
Figure 4. Size-dependent anodic dissolution of Pd-BCA NPs deposited on glassy carbon electrode in 0.1 M HClO₄ containing 10 mM NaCl at 1 mV/s under nitrogen. Bulk sample (in black), 100 kDa sample (in red), 30 kDa sample (in green), and 3 kDa sample (in magenta). Average particle size was 3.2 ± 0.9 , 1.5 ± 0.3 , and 1.0 ± 0.3 nm for 100, 30, and 3 kDa sample, respectively. Average particle size of bulk sample was 98 ± 38 nm.

the same electrode in fresh electrolyte; no peaks were observed during the second scan which confirms that all NPs dissolved completely during the first scan (see Supporting Information Figure S3 for LSVs). Control experiments were also done at a variety of surface coverage values to verify that the oxidation potential obtained from the LSV peak potentials was invariant with coverage—a requirement of the conditions delineated by Brainina.²¹ Figure S4 shows results of selected experiments. These results show a lack of coverage dependence in the low coverage range, with some evidence of coverage dependence at the highest coverages examined. Thus, only low coverage data were used in the samples statistically analyzed to obtain

oxidation potentials as a function of size. The strong dependence on chloride concentration necessitated care in preparation of solutions with precisely reproduced [Cl⁻]. Multiple scans were done on each sample to obtain statistically relevant values (shown in Table 1).

The data in Figure 4 clearly show dissolution peaks for Pd oxidation to PdCl₄²⁻ that are strongly size dependent. These are similar to the data previously reported for Ag and Au NPs.¹³⁻¹⁵ For the “bulk” sample, the oxidation peak appears at +0.70 V (black curve), consistent with expectations for bulklike behavior. This value was used in calculations of the effect of size on the potential shift away from the bulk value (see below). The lowest oxidation potential is observed at +0.34 V for the 1.0 ± 0.3 nm diameter NPs. This demonstrates a destabilization of these types of Pd NPs by over a third of a volt due to the small size of the 3 kDa sample. The scan for the 3 kDa sample (diameter 1.0 ± 0.3 nm) seems to show a smaller peak near the value expected for bulk Pd. This suggests that this sample may have contained a small fraction of much larger particles, perhaps due to aggregation at some point during sample processing.

The dissolution process is interpreted based on the predicted behavior for Pd dissolution to PdCl₄²⁻. The more rigorous analysis described by Tang and co-workers was not needed in the present case because the mechanism did not involve generation of a palladium oxide as part of the oxidation process.^{16,17} Dissolution of palladium is a two-electron process in the presence of chloride ions to form PdCl₄²⁻, as shown in eq 1. The redox potential (E_0) for this process is highly dependent on chloride ion concentration, as shown in eq 2.



$$E = E_0 - 2.303RT/nF \log[\text{Cl}^-]^4 \quad (2)$$

The oxidation potentials for the anodic dissolution process corresponding to Pd-BCA NPs of average size 3.2 ± 0.9 , 1.5 ± 0.3 , and 1.0 ± 0.3 nm were found to be 570 ± 12 , 467 ± 10 , and 343 ± 15 mV, respectively. As qualitatively predicted by the Plieth model and experimentally observed by Zamborini and co-workers for silver and gold nanoparticles, the present results show a size-dependent shift in oxidation potential for Pd NPs over the size range investigated.^{12–15}

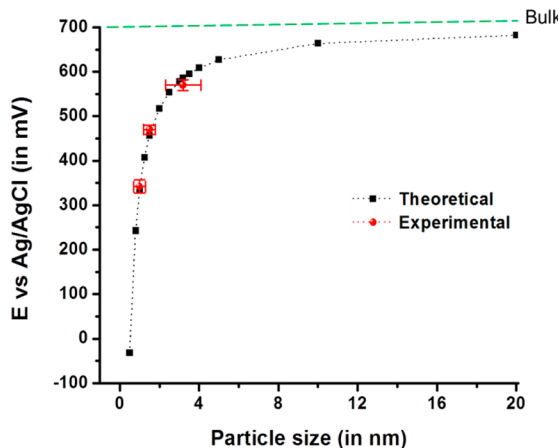


Figure 5. Experimentally observed oxidation potential for Pd-BCA NPs as a function of particle size (in red) and comparison with the theoretical values predicted by the Plieth model (in black).

Figure 5 shows a plot of the experimental oxidation potentials for BCA-Pd NPs as a function of NP radius, based on the model proposed by Plieth (eq 3):

$$\Delta E = E_{0,\text{Pd NP}} - E_{0,\text{bulk Pd}} = \frac{-2\gamma V_m}{zF} \frac{1}{r} \quad (3)$$

where $E_{0,\text{Pd NP}}$ is the oxidation potential of the variously sized BCA-Pd NPs, $E_{0,\text{bulk Pd}}$ is the oxidation potential of bulk Pd (i.e., the 0.70 V oxidation potential for the “bulk” >50 nm diameter Pd NP samples), γ is the surface energy of Pd (J m^{-2}), V_m is the molar volume of palladium ($\text{m}^3 \text{ mol}^{-1}$), z is the number of electrons, F is Faraday’s constant ($96485.34 \text{ C mol}^{-1}$), and r is the nanoparticle radius (m). The calculations used a surface energy value of bulk palladium of 2.0 J m^{-2} , as reported in the literature.^{40–42}

The plot shows an excellent fit of the data to the Plieth model using a value of the surface energy of 2.0 J m^{-2} . As for previous work on Pt, Au, and Ag, these anodic dissolution experiments reveal the intrinsic instability of very small metal NPs toward oxidation and dissolution. This will have substantial impact on any applications that require exposure of metal NPs to oxidizing potentials or oxidizing chemical conditions.

CONCLUSIONS

This study reports the synthesis of a new class of water-soluble Pd NPs. Capping with BCA endows the NPs with water solubility, an attractive feature. A simple purification procedure using centrifuge filters was developed to provide NPs with well-defined and narrow size distributions. Using these samples, a size-dependent shift in oxidation potential for anodic dissolution of Pd NPs was observed. The data are in excellent

agreement with a model proposed by Plieth. The purification strategy employed here can be used to obtain monodisperse nanoparticles of different sizes that can be used to examine the size dependence of catalytic activity—studies that are now underway.

ASSOCIATED CONTENT

S Supporting Information

TEM of bulk Pd-BCA NPs, TEM of Pd-BCA NPs synthesized under varying ligand and reducing agent conditions, LSV showing surface coverage control experiment, and Nafion control experiment. This material is available free of charge via the Internet at <http://pubs.acs.org>.

AUTHOR INFORMATION

Corresponding Author

*E-mail Dan.Buttry@asu.edu; Tel (480) 965-4430 (D.A.B.).

Notes

The authors declare no competing financial interest.

ACKNOWLEDGMENTS

We thank the electron microscopy laboratory in the ASU School of Life Sciences Bioimaging Facility for providing access to the TEM facility. We also acknowledge the use of HRTEM facilities within the LeRoy Erying Center for Solid State Science at Arizona State University. This material is based upon work supported by the National Science Foundation under Grant CHE-0957122.

REFERENCES

- Emory, S. R.; Haskins, W. E.; Nie, S. Direct Observation of Size-Dependent Optical Enhancement in Single Metal Nanoparticles. *J. Am. Chem. Soc.* **1998**, *120*, 8009–8010.
- Jain, P. K.; Huang, X.; El-Sayed, I. H.; El-Sayed, M. A. Noble Metals on the Nanoscale: Optical and Photothermal Properties and Some Applications in Imaging, Sensing, Biology, and Medicine. *Acc. Chem. Res.* **2008**, *41*, 1578–1586.
- Mulvaney, P. Surface Plasmon Spectroscopy of Nanosized Metal Particles. *Langmuir* **1996**, *12*, 788–800.
- Corma, A.; Garcia, H. Supported Gold Nanoparticles as Catalysts for Organic Reactions. *Chem. Soc. Rev.* **2008**, *37*, 2096–2126.
- McFarland, A. D.; Van Duyne, R. P. Single Silver Nanoparticles as Real-Time Optical Sensors with Zeptomole Sensitivity. *Nano Lett.* **2003**, *3*, 1057–1062.
- Nam, J. M.; Park, S. J.; Mirkin, C. A. Bio-Barcodes Based on Oligonucleotide-Modified Nanoparticles. *J. Am. Chem. Soc.* **2002**, *124*, 3820–3821.
- Keller, A. A.; Wang, H.; Zhou, D.; Lenihan, H. S.; Cherr, G.; Cardinale, B. J.; Miller, R.; Ji, Z. Stability and Aggregation of Metal Oxide Nanoparticles in Natural Aqueous Matrices. *Environ. Sci. Technol.* **2010**, *44*, 1962–1967.
- Zhang, H.; Gilbert, B.; Haung, F.; Banfield, J. F. Water Driven Structure Transformation in Nanoparticles at Room Temperature. *Nature* **2003**, *424*, 1025–1029.
- Chernavskii, P. A.; Peskov, N. V.; Mugtasimov, A. V.; Lunin, V. V. Oxidation of Metal Nanoparticles: Experiment and Model. *Russ. J. Phys. Chem. B* **2007**, *4*, 394–411.
- Sutter, E.; Sutter, P. Size-Dependent Room Temperature Oxidation of In Nanoparticles. *J. Phys. Chem. C* **2012**, *116*, 20574–20578.
- Li, X.; Lenhart, J. J. Aggregation and Dissolution of Silver Nanoparticles in Natural Surface Water. *Environ. Sci. Technol.* **2012**, *46*, 5378–5386.

- (12) Plieth, W. J. On The Electrochemical Properties of Small Clusters of Metal Atoms and Their Role in the Surface Enhanced Raman Scattering. *J. Phys. Chem.* **1982**, *86*, 3166–3170.
- (13) Zamborini, F. P.; Ivanova, O. S. Size-Dependent Electrochemical Oxidation of Silver Nanoparticles. *J. Am. Chem. Soc.* **2010**, *132*, 70–72.
- (14) Zamborini, F. P.; Ivanova, O. S. Electrochemical Size Discrimination of Gold Nanoparticles Attached to Glass/Indium-Tin-Oxide Electrodes by Oxidation in Bromide-Containing Electrolyte. *Anal. Chem.* **2010**, *82*, 5844–5850.
- (15) Masitas, R. A.; Zamborini, F. P. Oxidation of Highly Unstable < 4 nm Diameter Gold Nanoparticles 850 mV Negative of the Bulk Oxidation Potential. *J. Am. Chem. Soc.* **2012**, *134*, 5014–5017.
- (16) Tang, L.; Han, B.; Persson, K.; Friesen, C.; He, T.; Sieradzki, K.; Ceder, G. Electrochemical Stability of Nanometer-Scale Pt Particles in Acidic Environments. *J. Am. Chem. Soc.* **2010**, *132*, 596–600.
- (17) Tang, L.; Li, X.; Cammarata, R. C.; Friesen, C.; Sieradzki, K. Electrochemical Stability of Elemental Metal Nanoparticles. *J. Am. Chem. Soc.* **2010**, *132*, 11722–11726.
- (18) Ward Jones, S. E.; Campbell, F. W.; Baron, R.; Xiao, L.; Compton, R. G. Particle Size and Surface Coverage Effects in the Stripping Voltammetry of Silver Nanoparticles: Theory and Experiment. *J. Phys. Chem. C* **2008**, *112*, 17820–17827.
- (19) Kolb, D. M.; Englemann, G. E.; Ziegler, J. C. On the Unusual Electrochemical Stability of Nanofabricated Copper Clusters. *Angew. Chem., Int. Ed.* **2000**, *39*, 1123–1125.
- (20) Ng, K. H.; Liu, H.; Penner, R. M. Subnanometer Silver Clusters Exhibited Unexpected Electrochemical Metastability on Graphite. *Langmuir* **2000**, *16*, 4016–4023.
- (21) Brainina, K. Z.; Galperin, L. G.; Vikulova, E. V. Electrochemistry of Metal Nanoparticles: The Effect of Substrate. *J. Solid State Electrochem.* **2012**, *16*, 2357–2363.
- (22) Chen, S.; Huang, K. Electrochemical Studies of Water-Soluble Palladium Nanoparticles. *J. Cluster Sci.* **2000**, *11*, 405.
- (23) Zhao, W.; Gonzaga, F.; Li, Y.; Brook, M. A. Highly Stabilized Nucleotide-Capped Small Gold Nanoparticles with Tunable Size. *Adv. Mater.* **2007**, *13*, 1776–1771.
- (24) Singh, P.; Buttry, D. A. Comparison of Oxygen Reduction Reaction at Silver Nanoparticles and Polycrystalline Silver Electrodes in Alkaline Solution. *J. Phys. Chem. C* **2012**, *116*, 1056–10663.
- (25) Schmid, G.; Harms, M.; Malm, J. O.; Bovin, J. O.; Ruitenberg, J. V.; Zandbergen, H. W.; Fu, W. T. Ligand-Stabilized Giant Palladium Clusters: Promising Candidates in Heterogeneous Catalysis. *J. Am. Chem. Soc.* **1993**, *115*, 2046–2048.
- (26) Schmidt, T. J.; Gasteiger, H. A.; Stäb, G. D.; Urban, P. M.; Kolb, D. M.; Behm, R. J. Characterization of High-Surface-Area Electrocatalysts Using a Rotating Disk Electrode Configuration. *J. Electrochem. Soc.* **1998**, *145*, 2354–2358.
- (27) Teranishi, T.; Miyake, M. Size Control of Palladium Nanoparticles and Their Crystal Structures. *Chem. Mater.* **1998**, *10*, 594–600.
- (28) Lin, C. M.; Hung, T. L.; Huang, Y. H.; Wu, K. T.; Tang, M. T.; Lee, C. H.; Chen, C. T.; Chen, Y. Y. Size-Dependent Lattice Structure of Palladium Studied by X-Ray Absorption Spectroscopy. *Phys. Rev. B* **2007**, *75*, 125426–6.
- (29) Heinemann, K.; Poppe, H. In-Situ TEM Evidence of Lattice Expansion of Very Small Supported Palladium Particles. *Surf. Sci.* **1985**, *156*, 265–274.
- (30) Giorgio, S.; Henry, C. R.; Chapon, C.; Penisson, J. M. Structure and Morphology of Small Palladium Particles (2–6 nm) Supported on MgO Micro-Cubes. *J. Cryst. Growth* **1990**, *100*, 254–260.
- (31) Goyhenex, C.; Henry, C. R.; Urban, J. Measurements of the Lattice Parameter of Supported Palladium Clusters. *J. Philos. Mag., A* **1994**, *69*, 1073–1084.
- (32) Vermaak, J. S.; Mays, C. W.; Kuhlmann-Wilsdorf, D. On Surface Stress and Surface Tension: I. Theoretical Considerations. *Surf. Sci.* **1968**, *12*, 128–133.
- (33) Mays, C. W.; Vermaak, J. S.; Kuhlmann-Wilsdorf, D. On Surface Stress and Surface Tension: II. Determination of the Surface Stress of Gold. *Surf. Sci.* **1968**, *12*, 134–140.
- (34) Wassermann, H. J.; Vermaak, J. S. On the Determination of the Surface Stress of Copper and Platinum. *Surf. Sci.* **1972**, *32*, 168–174.
- (35) Montano, P. A.; Zhao, J.; Ramanathan, M.; Shenoy, G. K.; Schulze, W.; Urban, J. Structure of Silver Microclusters. *Chem. Phys. Lett.* **1989**, *164*, 126–130.
- (36) Jacobs, J. W.; Schryvers, D. S. A High-Resolution Electron Microscopy Study of Photodeposited Pd Particles on TiO₂ and Their Oxidation in Air. *J. Catal.* **1987**, *103*, 436–449.
- (37) Lamber, R.; Jaeger, N.; Schulz-Ekloff, G. Electron Microscopy Study of the Interaction of Ni, Pd and Pt with Carbon: II. Interaction of Palladium with Amorphous Carbon. *Surf. Sci.* **1990**, *227*, 15–23.
- (38) Kuhrt, C.; Anton, R. On the Origin of a Lattice Expansion in Palladium and Pd-Au Vapor Deposits on Various Substrates. *Thin Solid Films* **1991**, *198*, 301–315.
- (39) Xia, Y.; Xiong, Y.; Lim, B.; Skrabalak, S. E. Shape-Controlled Synthesis of Metal Nanocrystals: Simple Chemistry Meets Complex Physics? *Angew. Chem., Int. Ed.* **2008**, *48*, 60–103.
- (40) Qi, W. H.; Wang, M. P. Size and Shape Dependent Lattice Parameters of Metallic Nanoparticles. *J. Nanopart. Res.* **2005**, *7*, 51–57.
- (41) Redjala, T.; Remita, H.; Apostolescu, G.; Mostafavi, M.; Thomazeau, C.; Uzio, D. Bimetallic Au-Pd and Ag-Pd Clusters Synthesized by γ or Electron Beam Radiolysis and Study of the Reactivity/Structure Relationships in the Selective Hydrogenation of Buta-1,3-Diene. *Oil Gas Sci. Technol.* **2006**, *61*, 789–797.
- (42) Tyson, W. R.; Miller, W. A. Surface Free Energies of Solid Metals: Estimation from Liquid Surface Tension Measurements. *Surf. Sci.* **1972**, *62*, 267–276.